



DAMPING-DUCTILITY RELATIONSHIPS FOR THE DISPLACEMENT-BASED DESIGN OF FRICTION-SPRING FLAG-SHAPED STRUCTURES

N. Chan⁽¹⁾, A. Hashemi⁽²⁾, P. Zarnani⁽³⁾, P. Quenneville⁽⁴⁾

⁽¹⁾ Ph.D. candidate, University of Auckland, jcha367@aucklanduni.ac.nz

⁽²⁾ Postdoctoral Research Fellow, University of Auckland, a.hashemi@auckland.ac.nz

⁽³⁾ Lecturer, Auckland University of Technology, p.zarnani@aut.ac.nz

⁽⁴⁾ Professor, University of Auckland, p.quenneville@auckland.ac.nz

Keywords: damping-ductility; equivalent viscous damping; flag-shape; friction-spring; displacement-based design.

Abstract

The performance of structures is strongly correlated with the displacement that they undergo. Both structural and non-structural damage can be related to drift, which is one of the primary variables to control during seismic design. Due to the importance of displacement, a design approach based on the displacement of structures – i.e. Direct Displacement-Based Design (DDBD) – was developed and popularised by Priestley and colleagues in the 1990s. With this method, the designer can directly incorporate the target design displacement and energy dissipation into calculations.

For convenience of design, the reduction in the base-shear is usually quantified through an equivalent SDOF elastic model. The reason for this is that designers will be able to utilise an elastic SDOF response spectrum to obtain the likely response of their non-linear model, so long as the elastic model is equivalent to the non-linear one. In this sense, the word “equivalent” implies that the elastic model achieves an equivalent peak force and peak displacement as the non-linear one when subjected to the same excitation. To achieve this equivalence, the DDBD method employs the equivalent viscous damping parameter. This damping parameter is calibrated to ensure that the peak elastic response is equivalent to the non-linear one. The calibration process produces a damping-ductility relationship curve for the type of non-linear model. Designers can apply this relation to obtain an equivalent damping ratio to represent the energy dissipation, and to find the reduction in base shear. Since the resulting design base shear and cost is greatly influenced by this damping value, it is therefore imperative to ensure that the calibration process can be relied upon.

This paper details the development of damping-ductility laws for friction-spring dampers that possess flag-shaped load-deformation behaviour. These encourage structural members to re-centre to their original position upon unloading, thus minimising any residual deformation. Such re-centring systems are gaining popularity as there is increasing recognition of the severe consequences of residual drifts, which can result in demolishing the structure. Previous researchers have investigated damping-ductility laws for flag-shaped models, based on hysteretic parameters defined for very specific flag-shapes. However, recent innovations such as the Resilient Slip Friction Joint (RSFJ) allow for different flag-shapes that may not be adequately described by currently available curves. In this study, an expression of the damping ratio is derived which contains three key variables to describe and characterise any friction-spring model. These are the initial periods, the stiffness ratio for loading and the stiffness ratio for unloading. With these, damping-ductility curves can be produced for any similar system.

A set of 50 ground motions was used as the input excitation. From these, 300,000 damping-ductility data points were generated. To acquire each data point, optimisation algorithms were implemented in MATLAB to solve for the desired ductility value and its corresponding equivalent viscous damping ratio. MATLAB was used to perform the analyses and conduct the optimization algorithms. SAP2000 was used to verify the responses obtained. Results of the study indicate that parameters r_L and r_U play a major and minor role respectively on the damping ratio. The initial period becomes a significant factor at short-to-medium periods. The findings of this study give the most comprehensive damping-ductility relationship curves related to flag-shaped systems of friction-spring type. This can be used by researchers and practitioners when implementing the DDBD approach for optimised design of self-centring seismic resilient structures.



1. Introduction

The performance of structures is strongly correlated with the displacement that they undergo. Both structural and non-structural damage can be related to drift, which is one of the primary variables to control during seismic design. Due to the importance of displacement, a design approach based on the displacement of structures was developed and popularised by Priestley and colleagues in the 1990s. The Direct Displacement-Based Design (DDBD) method consists of four main steps [1], as illustrated in Fig. 1:

1. Specify a target displacement and estimate the yield displacement to obtain the target/desired ductility.
2. Approximate the multi-degree-of-freedom (MDOF) structure as an equivalent single-degree-of-freedom (SDOF) system.
3. For this target ductility and SDOF model, utilise an appropriate damping-ductility relationship to determine the amount of equivalent viscous damping.
4. Apply the damping ratio and target displacement to a damped elastic spectrum to obtain the effective period required. The base shear can then be obtained from this and from the mass.

In the final step of the DDBD method, the design base shear depends on the equivalent viscous damping ratio (EVDR) used. The EVDR represents a combination of elastic damping and hysteretic damping, which among other sources of dissipation, depends primarily on the type of energy dissipater employed. As this can have a significant impact on the outcome of the DDBD process, it is crucial to ensure that the damping-ductility law used in design is suitable and appropriate for the type of dissipater used. The scope of this paper covers the damping attributed to the hysteretic component of a friction-spring type damper.

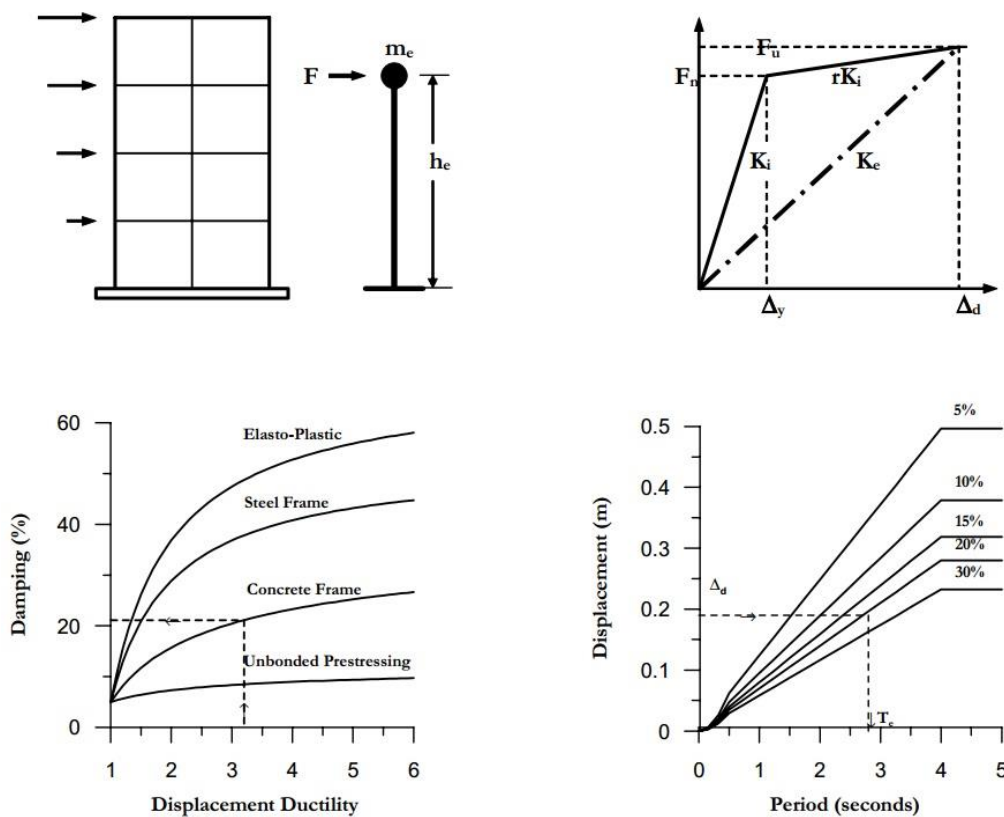


Fig. 1 – Four key steps of the Direct Displacement-Based Design (DDBD) process [2].



2. Currently Existing Equations

One means of quantifying the hysteretic damping is through an area-based method proposed by Jacobsen. The damping ratio is based on the proportion of area enclosed by a complete hysteresis loop, as Fig. 2 shows. For the specific type of flag-shape that friction-springs represent, the area-based expression was derived and presented in Eq. (1) as per notation in Fig. 2.

However, there are at least two disadvantages with Jacobsen's method. Firstly, Jacobsen derived this with a steady-state sinusoidal response so the appropriateness of this method to real earthquakes is debatable. Secondly, the method does not consider the structure's period, which is a key factor in any dynamic analysis and the resulting response.

Other researchers have proposed EVDR expressions that are related to the friction-spring behaviour. Blandon proposed Eq. (2), which applies only to one specific model with parameters $r_L = 0.04$ and $r_U = 0.875$ [2]. Dwairi proposed Eq. (3), which was obtained for a model with parameters $r_L = 0.10$ and $r_U = 0.40$ [3]. However, there is a need for an EVDR expression applicable to a wider range of r_L and r_U values that are possible with friction-springs. This paper attempts to fill that gap.

$$\xi_{hyst} = \frac{\mu - 1}{2\pi\mu} \left[\frac{(1 - r_L)(1 - r_U)}{(1 - r_L r_U)} \right] \left[\frac{r_L(\mu - 1) + 2}{r_L(\mu - 1) + 1} \right] \quad (1)$$

$$\xi_{eq} = \kappa \xi_{el} + 12.28 \left(1 - \frac{1}{\sqrt{\mu}} - \frac{\mu}{250} \right) \left(1 + \frac{1}{(T_e + 1)^3} \right) \quad (2)$$

$$\xi_{eq} = \begin{cases} \xi_{el} + [0.30 + 0.35(1 - T_e)] \left(\frac{\mu - 1}{\pi\mu} \right) & T_e \leq 1 \\ \xi_{el} + 0.30 \left(\frac{\mu - 1}{\pi\mu} \right) & T_e \geq 1 \end{cases} \quad (3)$$

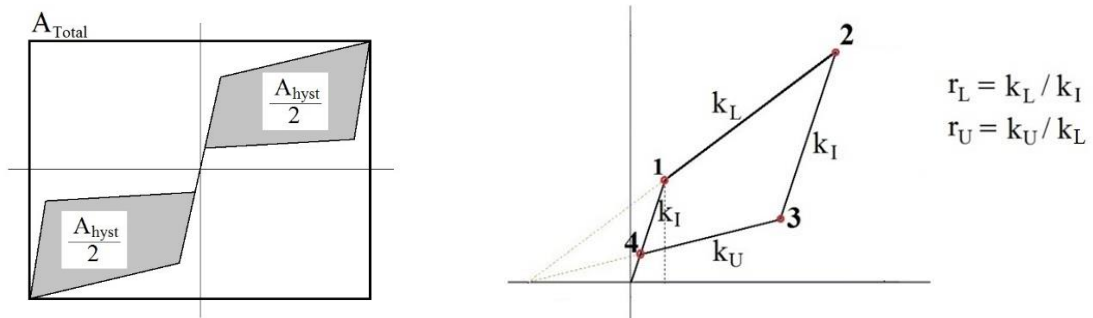


Fig. 2 – Left: Jacobsen's EVD calculated from the hysteretic (shaded) area. Right: Notation.

3. Friction-spring Hysteretic Model

Two examples of friction-spring dampers (Fig. 3) that are currently on the market are the German invention Ringfeder, and the more recent innovation RSFJ from New Zealand. Although they differ in form and in spring mechanism, one similarity that they do share is the use of tapered interfaces to induce wedging actions. Clamping pressure from the spring/wedging action varies with deformation, and so does the frictional resistance in proportion to the loading. Unlike flat friction plates, they are less prone to residual deformation and instead promotes re-centring.



This study examines the effect of three key parameters used to describe the friction-spring behaviour: the initial period T_i , the stiffness ratio r_L and the stiffness ratio r_U . The range of initial periods T_i span between 0.2 seconds to 2 seconds. Parameter r_L controls the loading or post-slip stiffness. Graphically, the limits are between perfectly-plastic behaviour ($r_L = 0$) and purely elastic behaviour ($r_L = 1$). Parameter r_U controls the unloading (re-centring) stiffness or energy dissipation. The limits are again at zero restoring force where maximum dissipation occurs ($r_U = 0$) and zero dissipation or multi-linear elastic behaviour ($r_U = 1$). Note that the ratio r_U has been defined slightly differently from other texts in literature. It is expressed as a ratio using the loading stiffness k_L rather than initial stiffness k_i because this allows limiting values of 0 and 1. Fig. 4 shows the effect of parameters r_L and r_U on the shape of the hysteresis.

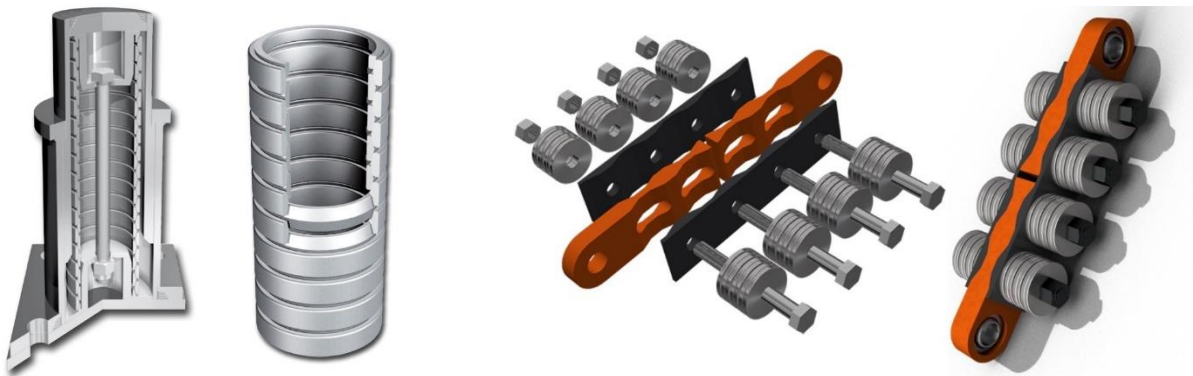


Fig. 3 – Commercially available friction-springs. Left: Ringfeder. Right: RSFJ.

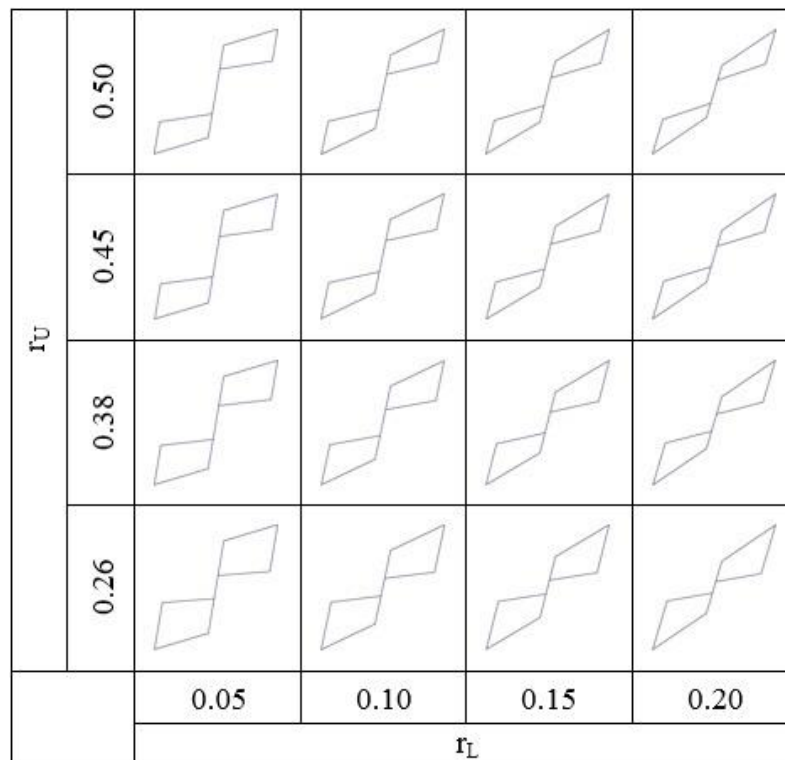


Fig. 4 – Range of values for parameters r_L and r_U and their effect on the hysteretic shape.



Analyses by Hill [4] and Hashemi [5] for the Ringfeder and the RSFJ respectively indicate that friction-spring hysteresis typically exhibits a larger loading stiffness than an unloading stiffness. This is due to the reversal of friction in loading/unloading. Based on that, the ratio r_U can be derived as:

$$r_U = \begin{cases} \gamma & \text{for the Ringfeder} \\ \gamma \frac{1}{r_L(\gamma - 1) + 1} & \text{for the RSFJ} \end{cases} \quad (4)$$

where

$$\gamma = \frac{\tan \alpha - \phi}{\tan \alpha + \phi} \frac{1 - \phi \tan \alpha}{1 + \phi \tan \alpha} \quad (5)$$

If the coefficient of friction ϕ is 0.15 (greased), the ratio r_U for the Ringfeder is typically 0.26 at a taper angle α of 14 degrees. For the RSFJ, the ratio r_U can vary from 0.26 to 0.50, as the taper angle varies from 15 degrees to 30 degrees. Angles below 15 degrees may hinder re-centring, and angles above 30 degrees may prevent slipping into the non-linear range. Hence, the values chosen for this study are $r_U = 0.26, 0.38, 0.45, 0.50$ which correspond to $\alpha = 15, 20, 25, 30$ degrees for the RSFJ. The r_L ratio is a function of the loading stiffness and the initial stiffness. There can be considerable variation in the initial stiffness, which depends on the elastic properties of the system. As such, the r_L ratios chosen are 0.05, 0.10, 0.15, 0.20 as a starting point for the analyses.

4. Method

In this parametric study, MATLAB code was initially used to perform the earthquake simulations and conduct the optimization algorithm. The simulations utilized a set of 50 ground motions, almost all of which were acquired from the NGA-West2 database. Time-history results were double-checked with the commercial software SAP2000. If any discrepancy arose which exceeded a strict tolerance, then SAP2000 would take over for that specific simulation. The process of obtaining damping-ductility data points is shown in Fig. 5 and Fig. 6, and can be described as follows:

1. Specify model values T_i , r_L , r_U . These give k_i , k_L and k_U for an arbitrary mass.
2. Select ground motion.
3. Select target ductility.
4. Find ground motion scale factor that produces the target ductility/displacement.
5. Find equivalent viscous damping ratio for the target displacement.
6. Repeat for all other ductilities (step 3), ground motions (step 2), and models (step 1).

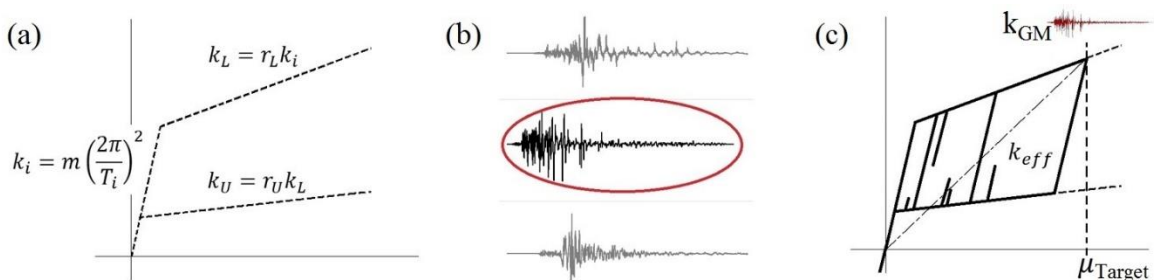


Fig. 5 – Illustration of procedure used to obtain damping-ductility data points.

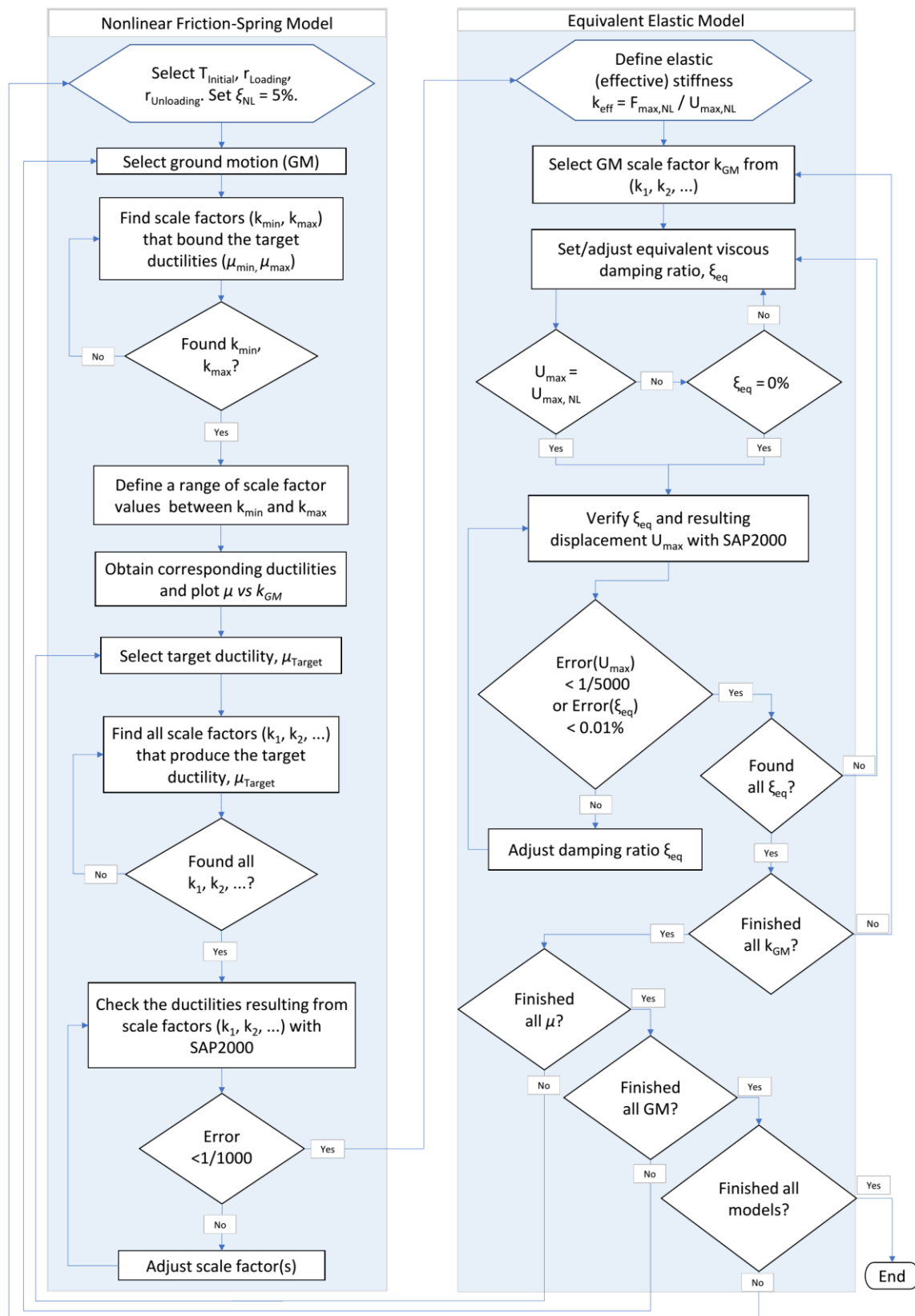


Fig. 6 – Flowchart depicting the main features of the MATLAB algorithm.

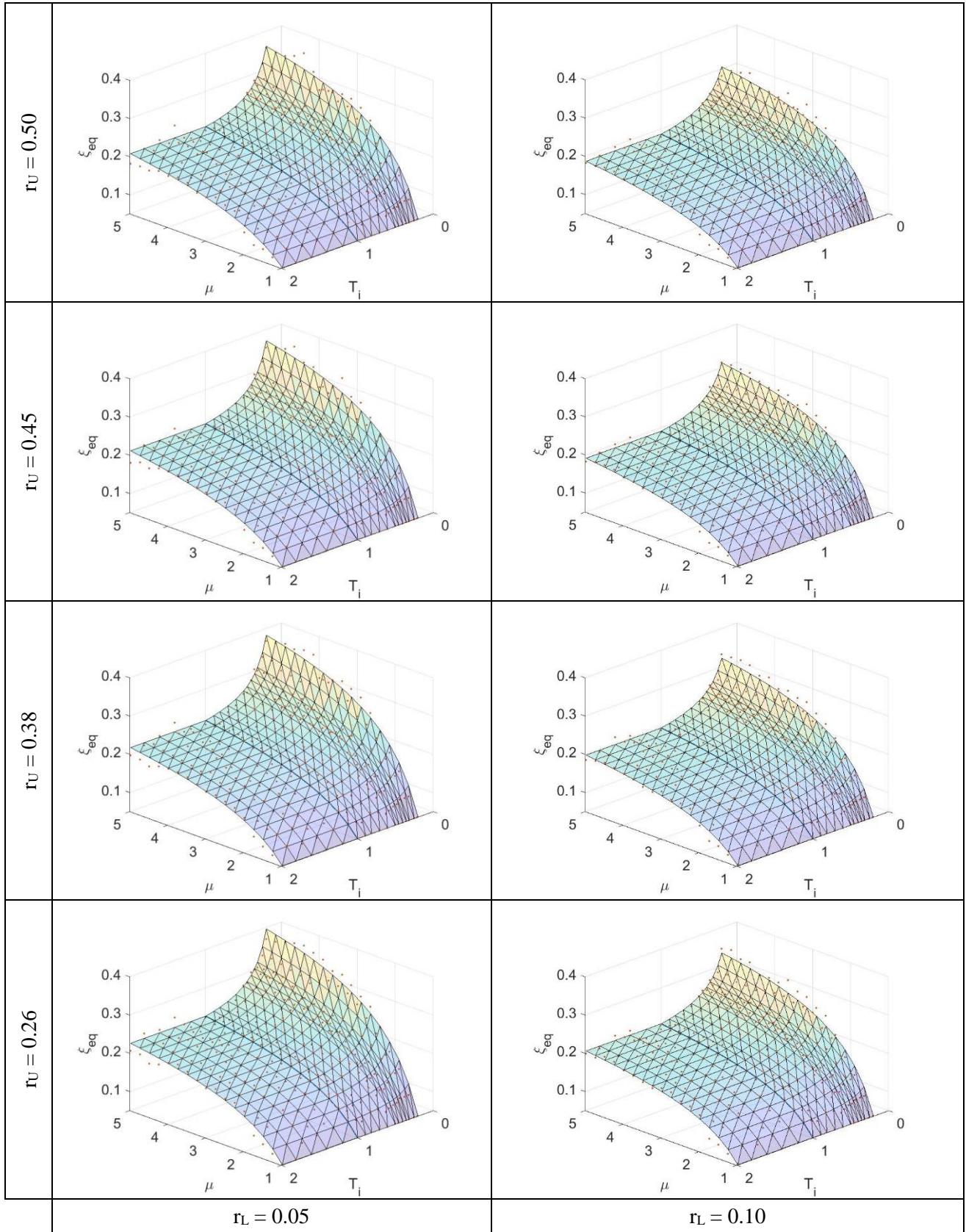


Fig. 7 – EVDR data points and fitted surface for $r_L = 0.05, 0.10$.

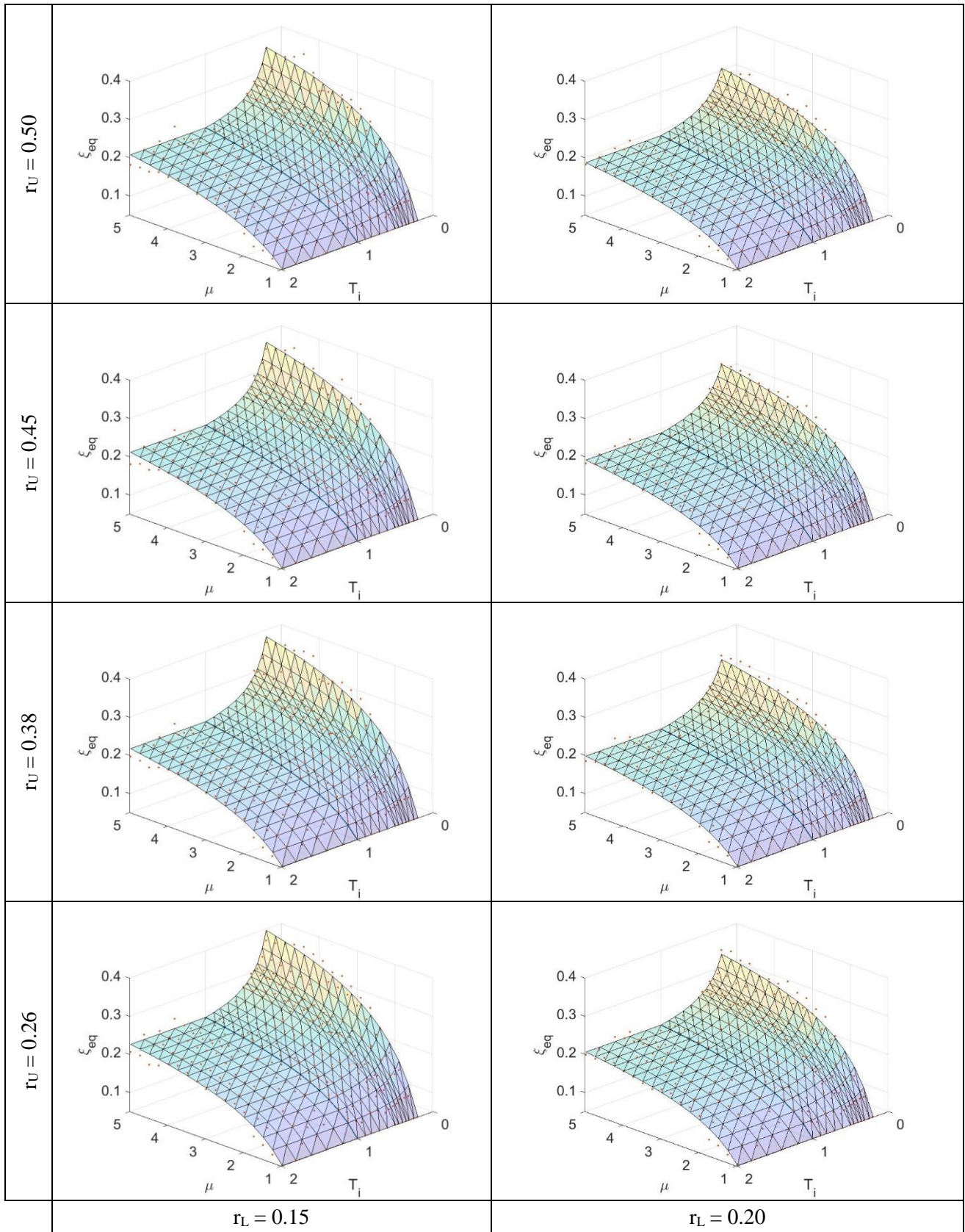


Fig. 8 – EVDR data points and fitted surface for $r_L = 0.15, 0.20$.



5. Results

Each data point in Fig. 7 and Fig. 8 represents the median of 50 damping ratios. A few trends are visible from these observations. Firstly, the damping ratios appear to show an inverse relationship with respect to r_L and r_U . For the range of r_L values considered, it is apparent that this parameter plays a major role on the resulting damping ratio. Although Khan [6] performed his study for thin Takeda models, he also observed that the post-yield stiffness ratio had a significant effect on the damping ratios, even more so than ground-motion variation.

On the other hand, parameter r_U has a smaller but noticeable impact on the damping ratio. However, this is only limited to the range of r_U examined; it may well have a larger effect over a wider range of values. Qualitatively speaking, the general trends due to r_L and r_U also agree with Jacobsen's method, whereby greater hysteretic areas result in higher damping ratios.

Secondly, the initial period also has an inverse effect across all 16 models. That is, the lower the initial period, the higher the damping ratios. This effect however is more pronounced between the short-to-medium period range, and gradually becomes negligible for longer periods.

6. Proposed EVDR Equations

The surface plots in Fig. 7 and Fig. 8 are generated from Eq. (6), which proposes a new expression of equivalent viscous damping ratios for the friction-spring damper. It is based on Priestley's exponential form which fits the data of concave growth.

In this model, there is an additional term to account for the effects of short-to-medium initial periods on the damping ratios. The coefficients for this equation, c_1 to c_5 depend on the model characteristics. They are expressed in terms of the ratios r_L and/or r_U . Coefficients c_1 to c_4 are polynomial functions and can be calculated via Eq. (7) and the coefficients in Tables 1 to 4. Coefficient c_5 is merely a linear function of r_L .

$$\xi_{eq} = \begin{cases} 0.05 + c_1 \left(1 - \frac{1}{\mu^{c_2}}\right) + c_3 \left(1 - \frac{1}{\mu^{c_4}}\right) \left(\frac{1}{T_i^{c_5}} - 1\right) & \text{for } T_i \leq 1 \text{ sec} \\ 0.05 + c_1 \left(1 - \frac{1}{\mu^{c_2}}\right) & \text{for } T_i \geq 1 \text{ sec} \end{cases} \quad (6)$$

where

$$c_n = \begin{cases} \sum a_{ij(n)} r_L^i r_U^j & \text{for } n = 1 \text{ to } 4 \\ 1.2 - 4r_L & \text{for } n = 5 \end{cases} \quad (7)$$

Table 1 – Coefficients of the polynomial function for c_1 .

n = 1	r_L^0	r_L^1	r_L^2	r_L^3
r_U^0	5.500819	-250.337	2453.501	-6689.23
r_U^1	-38.2239	1935.702	-19169.2	52417.41
r_U^2	88.13942	-4743.28	47489.63	-130476
r_U^3	-53.5534	3545.186	-36809.2	102647.6

Table 2 – Coefficients of the polynomial function for c_2 .

$n = 2$	r_L^0	r_L^1	r_L^2	r_L^3
r_U^0	-18.0245	643.7033	-5839.8	15548.78
r_U^1	147.717	-5115.69	46315.33	-123192
r_U^2	-383.321	13120.87	-118238	314155.8
r_U^3	321.1454	-10951.3	98437.66	-261353

Table 3 – Coefficients of the polynomial function for c_3 .

$n = 3$	r_L^0	r_L^1	r_L^2	r_L^3
r_U^0	0.099213	-0.5299	2.443428	0
r_U^1	-0.11816	0.508016	0	0
r_U^2	0.034929	0	0	0
r_U^3	0	0	0	0

Table 4 – Coefficients of the polynomial function for c_4 .

$n = 4$	r_L^0	r_L^1	r_L^2	r_L^3
r_U^0	-0.65987	14.45854	-13.218	0
r_U^1	3.67023	-10.1987	0	0
r_U^2	-0.97186	0	0	0
r_U^3	0	0	0	0

An example follows to calculate the damping-ductility curve of a given model. For a model with parameters:

$$r_L = 0.05$$

$$r_U = 0.26$$

$$T_i = 0.40 \text{ sec}$$

The long-period curve for this model is obtained from constants c_1 and c_2 :

$$\begin{aligned} c_1 &= 5.5 - 250r_L - 38.2r_U + 1935r_Lr_U + \dots + 102648r_L^3r_U^3 \\ &= 0.3826 \end{aligned}$$

$$\begin{aligned} c_2 &= -18 + 644r_L + 148r_U - 5116r_Lr_U + \dots - 261353r_L^3r_U^3 \\ &= 0.3885 \end{aligned}$$

Since the specified initial period T_i is under 1 sec, an adjustment uses additional constants c_3 to c_5 :

$$\begin{aligned} c_3 &= 0.099 - 0.530r_L - 0.118r_U + 0.508r_Lr_U + 2.443r_L^2 + 0.0349r_U^2 \\ &= 0.0571 \end{aligned}$$



$$\begin{aligned} c_4 &= -0.66 + 14.46r_L + 3.67r_U - 10.20r_L r_U - 13.22r_L^2 - 0.97r_U^2 \\ &= 0.7860 \end{aligned}$$

$$\begin{aligned} c_5 &= 1.2 - 4r_L \\ &= 1 \end{aligned}$$

These give the damping-ductility curve for the specified model:

$$\begin{aligned} \xi_{eq} &= 0.05 + c_1 \left(1 - \frac{1}{\mu^{c_2}}\right) + c_3 \left(1 - \frac{1}{\mu^{c_4}}\right) \left(\frac{1}{T_i^{c_5}} - 1\right) \\ &= 0.05 + 0.3826 \left(1 - \frac{1}{\mu^{0.3885}}\right) + 0.0571 \left(1 - \frac{1}{\mu^{0.786}}\right) \left(\frac{1}{T_i} - 1\right) \end{aligned}$$

One caveat is that further analyses at extremely high ductilities seem to indicate that the curve begins to fall, but this will not be shown here as further study is required to understand the cause(s) and condition(s) behind this. Caution is also advised when attempting to apply this equation outside the range of values studied in this paper.

7. Conclusions

The goal of this study is to produce damping-ductility relationships for flag-shaped models of friction-spring type. Key parameters used to describe a friction-spring model are the initial period T_i , the initial-to-loading stiffness ratio r_L and the loading-to-unloading stiffness ratio r_U . The range of values studied include T_i from 0.2 seconds to 2 seconds; r_L from 0.05 to 0.20; and r_U from 0.26 to 0.50. A derivation of the parameter r_U for commercially available friction-springs provides a practical basis for the chosen values.

Parametric analyses subjected these models to a set of 50 amplitude-scaled ground motions. It produced 300,000 individual damping-ductility data points. Each data point was the result of numerous iterations to satisfy strict tolerances imposed. From these, regression analyses produced a new expression for the equivalent viscous damping ratio in Eq. (6).

The proposed equation indicates that the initial period has a strong influence on the damping-ductility curve. This is especially so at short periods, which have the highest damping ratios across all models. Smaller values for parameters r_L and r_U also lead to an increase in the damping ratios, with r_L having a major effect and r_U having a minor effect for the range of values studied. This trend was expected and a similar observation of the significance of r_L was also found in a study on the thin-Takeda hysteresis [6].

The results of this study offer a flexible damping-ductility formula that can be used on a relatively wide range of friction-spring systems. This can be used by researchers and practitioners when implementing the Direct Displacement-Based Design approach for the design of self-centring seismically resilient structures.

Acknowledgements

The authors would like to acknowledge the Center for eResearch at the University of Auckland which provided the computing resources for this study.



References

- [1] Priestley MJN, Grant DN (2005): Viscous damping in seismic design and analysis. *Journal of Earthquake Engineering*, 9:sup2, 229-255.
- [2] Blandon CA, Priestley MJN (2005): Equivalent viscous damping equations for direct displacement-based design. *Journal of Earthquake Engineering*, 9:sup2, 257-278.
- [3] Dwairi HM, Kowalsky MJ, Nau JM (2007): Equivalent damping in support of direct displacement-based design. *Journal of Earthquake Engineering*, 11:4, 512-530.
- [4] Hill KE (1995): The utility of ring springs in seismic isolation systems. *Ph.D. Thesis*. Department of Mechanical Engineering, University of Canterbury, Christchurch, New Zealand.
- [5] Hashemi A, Zarnani P, Masoudnia R, Quenneville JHP (2017): Seismic resistant rocking coupled walls with innovative Resilient Slip Friction (RSF) joints. *Journal of Constructional Steel Research*, 129: 215–26.
- [6] Khan E, Kowalsky MJ, Nau JM (2016): Equivalent viscous damping model for short-period reinforced concrete bridges. *Journal of Bridge Engineering*, 21(2).